Organisation of human ER-exit sites: requirements for the localisation of Sec16 to transitional ER

Helen Hughes[1,*], Annika Budnik[1,*], Katy Schmidt[1,*], Krysten J. Palmer[1], Judith Mantell[1,3], Chris Noakes[1,‡], Andrew Johnson[1,§], Deborah A. Carter[3], Paul Verkade[1,2,3], Peter Watson[1,¶] and David J. Stephens[1,]**

[1]Cell Biology Laboratories, Department of Biochemistry, [2]Department of Physiology and Pharmacology and [3]Wolfson Bioimaging Facility, University of Bristol School of Medical Sciences, University Walk, Bristol BS8 1TD, UK

*These authors contributed equally to this work
‡Present address: Faculty of Life Sciences, University of Manchester, Oxford Road, Manchester M13 9PL
§Present address: Sir William Dunn School of Pathology, University of Oxford, South Parks Road, Oxford OX1 3RE
¶Present address: School of Biosciences, Cardiff University, Cardiff CF10 3AX, UK
**Author for correspondence (david.stephens@bristol.ac.uk)

Accepted 18 May 2009
Journal of Cell Science 122, 2924-2934 Published by The Company of Biologists 2009
doi:10.1242/jcs.044032

Summary

The COPII complex mediates the selective incorporation of secretory cargo and relevant machinery into budding vesicles at specialised sites on the endoplasmic reticulum membrane called transitional ER (tER). Here, we show using confocal microscopy, immunogold labelling of ultrathin cryosections and electron tomography that in human cells at steady state, Sec16 localises to cup-like structures of tER that are spatially distinct from the localisation of other COPII coat components. We show that Sec16 defines the tER, whereas Sec23-Sec24 and Sec13-Sec31 define later structures that precede but are distinct from the intermediate compartment. Steady-state localisation of Sec16 is independent of the localisation of downstream COPII components Sec23-Sec24 and Sec13-Sec31. Sec16 cycles on and off the membrane at a slower rate than other COPII components with a greater immobile fraction. We define the region of Sec16A that dictates its robust localisation of tER membranes and find that this requires both a highly charged region as well as a central domain that shows high sequence identity between species. The central conserved domain of Sec16 binds to Sec13 linking tER membrane localisation with COPII vesicle formation. These data are consistent with a model where Sec16 acts as a platform for COPII assembly at ERES.

Supplementary material available online at
http://jcs.biologists.org/cgi/content/full/122/16/2924/DC1

Key words: COPII, Membrane traffic, Secretion, Vesicle formation

Introduction

The first step of the mammalian secretory pathway is the export of proteins from the ER (reviewed by Hughes and Stephens, 2008). The accumulation of secretory cargo, deformation of the membrane and formation of transport vesicles is mediated by the COPII coat complex. In the yeast *Pichia pastoris* and metazoans, COPII assembly occurs at discrete sites on the ribosome-free ER, previously termed transitional ER (tER) or ER exit sites (ERES) (Palade, 1975; Orci et al., 1991; Bannykh et al., 1996; Tang et al., 2005). ERES is a term variously used in the literature and can best be defined as encompassing the tER membrane along with any post-ER structures up to (and according to the definition used by some, including) the ER-Golgi intermediate compartment (ERGIC) (Appenzeller-Herzog and Hauri, 2006). The classical distribution of COPII-coated ERES, as observed by light microscopy and immunoelectron microscopy, shows them to be distributed throughout the cell cytoplasm, clustering in the juxtanuclear area of cell types with a juxtanuclear Golgi (Orci et al., 1991; Bannykh et al., 1996; Martinez-Menarguez et al., 1999; Hammond and Glick, 2000; Stephens et al., 2000). The juxtanuclear ERES population accounts for 50-60% of ERES within the cell; intriguingly, some data exists that even suggests the possibility of membrane connectivity between ERES and Golgi (Sesso et al., 1992; Stinchcombe et al., 1995; Ladinsky et al., 1999).

COPII assembly is triggered by GDP-GTP exchange on the small GTP-binding protein Sar1. This step is catalysed by the Sec12 guanine nucleotide exchange factor, which in humans, localises throughout the ER membrane (Weissman et al., 2001) (D.J.S., unpublished observations). This results in the sequential assembly of Sec23-Sec24 [which provides the major cargo-binding capacity of the coat (Miller et al., 2002)] and Sec13-Sec31, which assembles around the nascent vesicle and acts to trigger high levels of GTPase activity on Sar1 to complete scission (Bielli et al., 2005; Lee et al., 2005; Sato and Nakano, 2005; Townley et al., 2008). Our data has suggested that Sec16 is recruited in a Sar1-dependent manner, because the expression of a GDP-restricted mutant (albeit at very high levels) results in delocalisation of Sec16 from ERES (Watson et al., 2006). Recent data from studying the *Drosophila* Sec16 protein suggests a different mechanism in which Sec16 acts as a spatial platform to concentrate Sar1 in its GTP-bound form following its activation to the GTP-bound state by Sec12 (Ivan et al., 2008).

The mechanism by which COPII assembly is restricted to transitional ER in metazoans remains largely unclear. Recent advances have been made in this area through the identification of orthologues of Sec16, an essential protein for COPII vesicle formation in the yeast *Saccharomyces cerevisiae* (Espenshade et al., 1995). In *S. cerevisiae*, COPII complexes form stochastically at sites across the entire ER membrane, with no apparent spatial organisation of budding. By contrast, in another yeast, *P. pastoris*, COPII assembly is organised in a manner dependent on Sec16 (Connerly et al., 2005). Identification of metazoan orthologues of Sec16 (Watson et al., 2006; Bhattacharyya and Glick, 2007; Iinuma et al., 2007; Ivan et al., 2008) has provided further insight in to the spatial restriction of COPII assembly in cells.

In humans, there are two genes that encode the Sec16 orthologues Sec16A and Sec16B. Sec16A can be seen as the primary orthologue as it is most similar (at ~240 kDa, notably in size) to Sec16 in other species. In *P. pastoris*, Sec16 is present at ERES at a concentration that is an order of magnitude lower than that of COPII subunits; as a result of this, Sec16 is suggested to be a modulator of COPII function rather than a stoichiometric subunit of the COPII coat (Connerly et al., 2005). In addition, COPII vesicle budding can be reconstituted in vitro in the absence of Sec16 (Matsuoka et al., 1998) consistent with a role in spatial organisation or regulation of COPII function rather than budding per se.

When Sec16A is expressed at high levels in HeLa cells, it results in the loss of other COPII subunits (Sec23-Sec24 and Sec13-Sec31) from the membrane (Watson et al., 2006). Although Sec16A is known to cycle on and off the membrane at ERES (Watson et al., 2006), the rate of recovery of fluorescence (i.e. the rate of recycling on and off the membrane) has not been accurately determined in comparison with COPII coat proteins. The human orthologue of Sec16 has been shown to bind Sec23 (Bhattacharyya and Glick, 2007) and its localisation to tER is dictated by a short, relatively poorly conserved, region just upstream of a central conserved domain (CCD). This CCD shows quite a high level of conservation between species (Bhattacharyya and Glick, 2007). In contrast to this, the *Drosophila* orthologue of Sec16 appears to require both this highly charged region, as well as the CCD for correct targeting to tER (Ivan et al., 2008). Here, we define the precise subcellular localisation of mammalian Sec16 relative to other COPII components. We also identify a region that specifies localisation of the protein to ERES and also interacts with Sec13.

Results

Localisation of COPII proteins by light microscopy

We sought to determine the spatial distribution of Sec16 and other components of ERES using light microscopy. Cells expressing a very low level of GFP-Sec16A were immunolabelled with antibodies specific to Sec24C, Sec31A, ERGIC-53 and COPI. Fig. 1A (enlarged in Fig. 1B) shows cells expressing GFP-Sec16A (green) that have been fixed and labelled for Sec24C (red) and ERGIC-53 (blue), or in Fig. 1C, enlarged in Fig. 1D, Sec31A (red) and β′-COP (blue). Individual ERES at high magnification are also shown (Fig. 1C, enlarged in Fig. 1D). Cells were imaged at the highest spatial resolution allowed by conventional laser-scanning confocal microscopy, satisfying Nyquist criteria and ensuring that no pixels were saturated. In these images, the discrete localisation of each component is clearly seen: with close juxtaposition but clear spatial separation of Sec16A from Sec24C and Sec31A. By contrast, Sec24C and Sec31A show almost complete colocalisation under these conditions (Fig. 1E,F). This offset occurs in >80% of ERES. Both Sec16A-positive structures and Sec24C- or Sec31A-positive structures were distinct from those labelled with ERGIC-53, as is expected (Hughes and Stephens, 2008). Some overlap was evident, consistent with potential colocalisation and interaction of these proteins. Indistinguishable results were obtained using GFP-Sec16B and also endogenous Sec16A using anti-Sec16A (KIAA0310) (data not shown). The localisation of endogenous Sec16A was then further defined using immunoelectron microscopy.

Sec16A and COPII outer subunit Sec31A rarely colocalise but appear in distinct clusters

Immunogold labelling of ultrathin cryosections and electron microscopy was undertaken to define the spatial arrangement of these protein clusters at the ultrastructural level. Here we studied endogenous Sec16A in combination with other proteins using an antibody previously characterised for this technique (Ronchi et al., 2008). In most cases Sec16A and Sec31A labelling were observed at a distance of between 100 nm and 600 nm apart (Fig. 2A, quantified in Fig. 2B); this is entirely consistent with our light microscopy data. Sec16A labelling tends to form clusters as judged by multiple gold particles seen together, whereas Sec31A labelling is usually observed alone or in small groups (rarely more than four gold particles); this could reflect the efficiency of labelling which could be reduced by oligomerisation of Sec31A in to a cage structure (Stagg et al., 2006). Indistinguishable results were obtained when, to control the quantification and exclude effects of differential staining efficiency, gold particle sizes were swapped for secondary antibodies in a separate experiment and counted the same way (data not shown). Membrane localisation of Sec16A was seen in 69% of structures (706 of 1028 gold particles), and in 20% of cases, we observed clear localisation of Sec16 to cup-like structures (45 of 223 Sec16A-positive structures), such as those shown in the upper panels of Fig. 2C. In double labelling experiments, 14% of Sec16A-labelled structures showed colocalisation of Sec16A with Sec31A (28 of 199 Sec16A-labelled structures). The typical size of an ERES has been defined as around 400 nm (Bannykh et al., 1996;

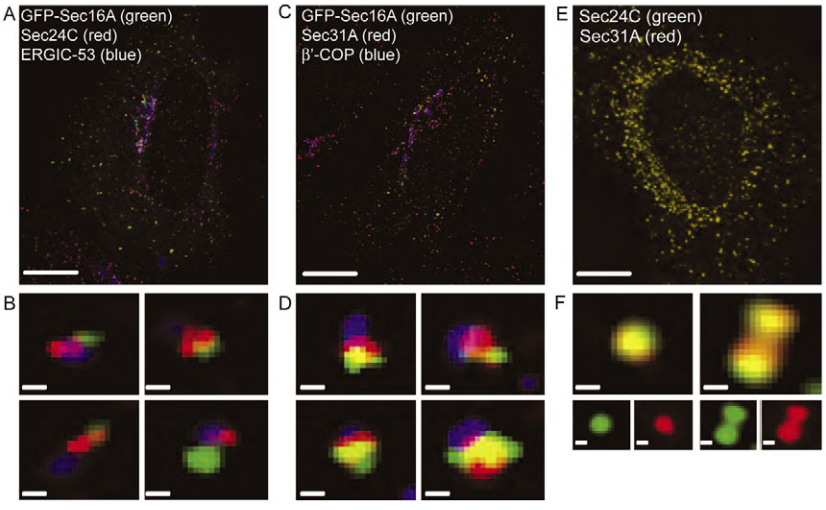

Fig. 1. Localization of GFP-Sec16A, COPII subunits and ERGIC components. (A,B) HeLa cells transfected with GFP-Sec16A fixed after 22 hours, stained with antibodies to the COPII subunit Sec24C and the ERGIC marker ERGIC-53. (C,D) HeLa cells transfected with GFP-Sec16A fixed after 22 hours and stained with antibodies to the COPII subunit Sec31A and the COPI subunit β′-COP. The images were taken using high resolution laser-scanning confocal microscopy, and images underwent iterative deconvolution. (E,F) HeLa cells fixed and stained with antibodies to Sec23A and Sec31A, showing complete colocalisation between COPII proteins. Enlarged images from the panels above are shown in B,D,F. Scale bars: 5 μm (A,C,E); 100 nm (B,D,F).

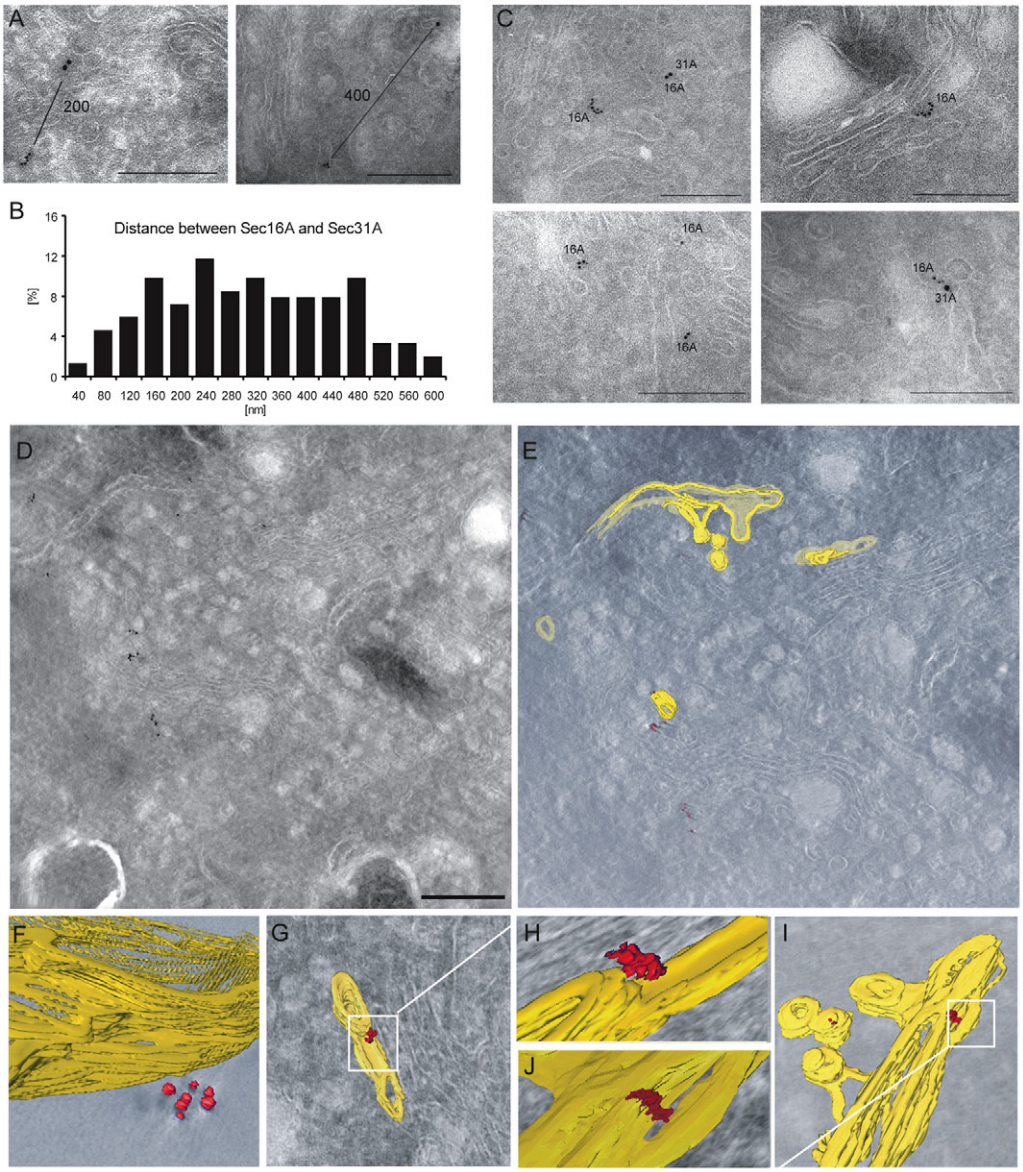

Fig. 2. Sec16A and Sec31A immunoelectron microscopy. (A-C) Localisation of Sec16A and Sec31A by immunogold labelling of ultrathin cryosections. Sec16A (6 nm gold particles) and Sec31A (10 nm gold particles) were immunolocalised on cryosections of HeLa cells. (A) Examples of measurement of distance between Sec16A and Sec31A. (B) Quantification of distance of gold grains from three independent experiments, taken from 74 images of juxtanuclear areas of HeLa cells. (C) Colocalisation with Sec31A, membrane association and cup-shaped labelling pattern for Sec16A. Scale bars: 200 nm. (D-J) Electron tomography of Sec16-labelled structures. (D) Sec16A immunolocalisation on a 210 nm cryosection in electron tomography. Image shows four merged orthoslices. (E) Example from the transparency projection. ER membrane in yellow, Sec16A label in red. (F) Magnified image showing association of Sec16A with membrane structures from a different tomogram. (G,H) Rotated magnifications of one Sec16 cluster; (I,J) Rotated magnifications of a distinct cluster (both from the data set in D,E). Scale bar: 200 nm.

Zeuschner et al., 2006). Thus, it is possible the measurements we made that show distances separating Sec16 and Sec31 labelling of >400 nm (and up to 600 nm) in fact represent labelling from two discrete ERES.

To better define the nature of these cup-shaped structures, we undertook electron tomography on ~210-nm-thick cryosections that were immunolabelled with antibodies directed against Sec16A (Fig. 2D-I; supplementary material Movie 1). Fig. 2A shows an example of gold labelling of Sec16A on four merged orthoslices. Membranes directly connected to areas of Sec16A labelling were traced and used to generate a 3D reconstruction of the section (Fig. 2E, traced membranes are shown in yellow with gold particles in red). Enlargements of these areas showed that Sec16 associates with both flat (Fig. 2F) and curved structures (Fig. 2G, further enlarged in Fig. 2H; Fig. 2I, enlarged in Fig. 2J). Both structures seen in Fig. 2H,J are consistent with concave surfaces contiguous with underlying ER membrane. We were unable to determine whether the more spherical membrane structures in Fig. 2H are ER tubules in section (which is our favoured interpretation) or budding (or even free) vesicles; this will require further investigation using multiple labelled sections and perhaps alternative labelling methodologies. A key limitation at present is the restriction of label to the surface of thick sections, which prevents a clear analysis of all COPII labelling.

Kinetics of association of Sec16A at tER

The kinetics of membrane association of COPII proteins at individual tER sites have previously been shown to occur on the scale of a few seconds (Sato and Nakano, 2005; Forster et al., 2006), in accordance with in vitro data (Antonny et al., 2001). To accurately determine whether Sec16A has the same cycling rate as other COPII subunits, and whether a substantial proportion of Sec16 could remain associated with the membrane to act as a platform for COPII assembly (Watson et al., 2006; Fromme et al., 2007; Heinzer et al., 2008; Ivan et al., 2008), fluorescence recovery after photobleaching (FRAP) experiments were undertaken and data fitted to a single exponential as described previously (Forster et al., 2006). Fig. 3 shows FRAP data for both

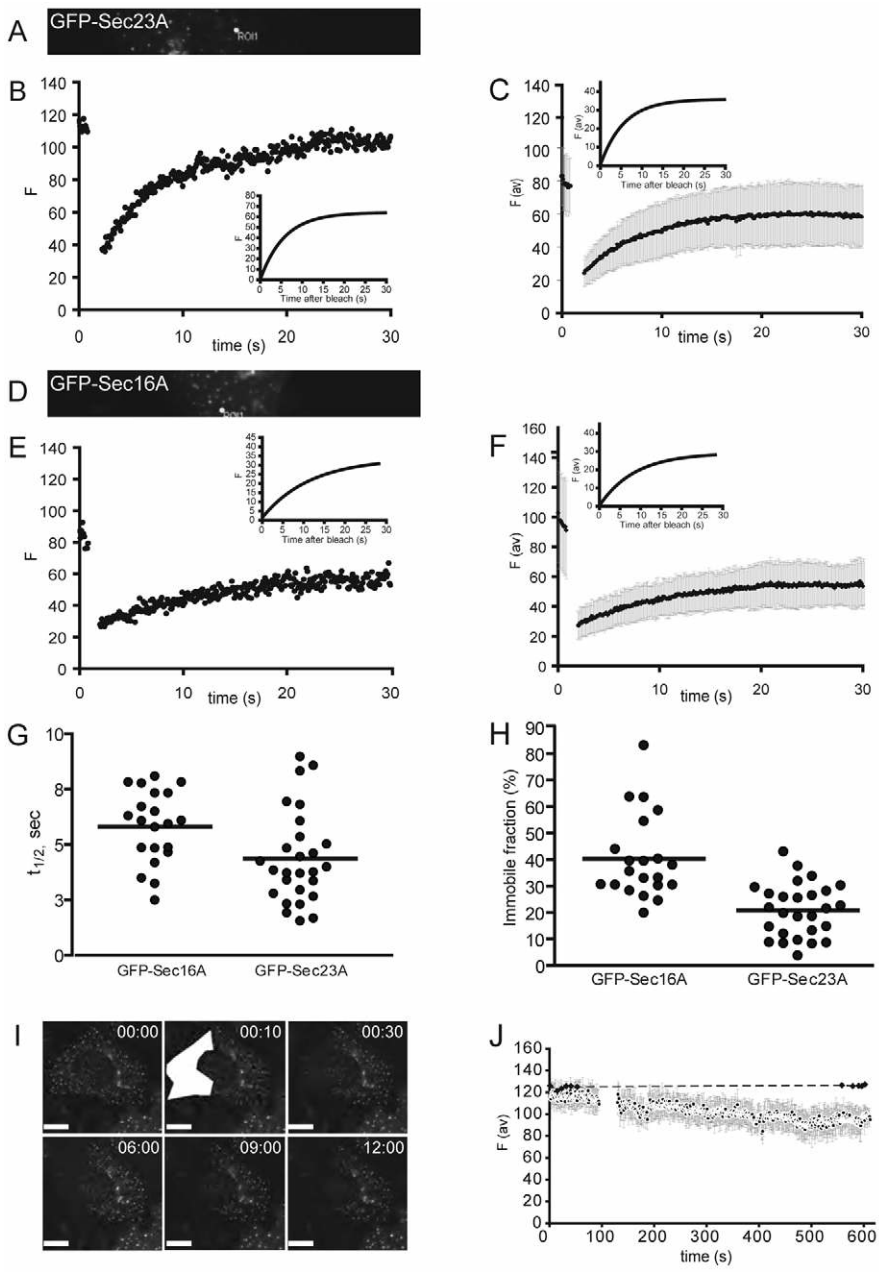

Fig. 3. Fluorescence photobleaching of GFP-Sec16A and GFP-Sec23A at ERES. (A-C) FRAP using GFP-Sec23A, (D-F) or GFP-Sec16A. Panels show the region of interest used for photobleaching (circled) for GFP-Sec23A (A) and GFP-Sec16A (D). (B,E) An example plot from a single ERES is shown; the insets show these data fitted to a single exponential. For GFP-Sec23A (C) and for GFP-Sec16A (F) data from ERES were averaged and plotted (error bars show s.d., n=21 for GFP-Sec16A and n=27 for GFP-Sec23A); insets show these data fitted to a single exponential. Individual recovery rates (G) and immobile fractions (H) were plotted. Data shown represent the mean of at least 16 independent experiments (horizontal bar). (I) HeLa cells expressing GFP-Sec16A were repeatedly bleached within a region of interest indicated in panel 2 (t=10 seconds), at 37°C followed by imaging the entire field of view at low laser power. (J) Mean fluorescence intensities (±s.d.) of nine ERES are plotted. This example is representative of a data set of six different cells, and for time courses of both 12 minutes and 30 minutes. After repeated bleaching, GFP-Sec16A-labelled ERES outside the ROI showed a slow loss in fluorescence (black circles) relative to no loss in fluorescence as seen for ERES of neighbouring cells (grey squares). F, fluorescence intensity; F(av), average fluorescence intensity, both in arbitrary units.

GFP-Sec23A (Fig. 3A-C) and GFP-Sec16A (Fig. 3D-F) including sample images of ERES used for defining the bleach region of interest (Fig. 3A,D), example curves obtained from individual ERES (Fig. 3B,E where the insets show these data fitted to a single exponential) and averaged data from multiple ERES (Fig. 3C,F, including insets, where these averaged data have been fitted to a single exponential). In good agreement with previously published data (Forster et al., 2006), GFP-Sec23A recycled with an average half-life of recovery of 4.36±0.40 seconds compared with GFP-Sec16A, where the average rate of recycling was 5.81±0.36 seconds (Fig. 3G). This difference, although small, was statistically significant (P=0.0098). The immobile fraction (i.e. the protein that remains bound to the membrane during post-bleach cycles, thus not exchanging with a mobile pool), was also different for both proteins; the average immobile fraction of Sec16A was 43±4.52%, which was significantly higher (P<0.0001) than that observed for Sec23A (21.8±1.94%) (Fig. 3H). Thus, a greater proportion of Sec16A is immobile on the tER membrane compared with Sec23A. Our FRAP experiments were undertaken on a relatively short timescale and so it is possible that this immobile fraction is in fact simply turning over very slowly. Thus, we undertook fluorescence loss in photobleaching experiments using GFP-Sec16A to investigate this further. Fig. 3I shows images of cells which have undergone iterative cycles of high intensity bleaching within the designated region of interest and low intensity imaging of ERES. Analysis of the fluorescence intensity of individual ERES outside of bleach regions in these experiments (Fig. 3J) showed a slow steady decline in fluorescence intensity. We conclude that the immobile fraction detected in FRAP experiments is indeed that, and that it does not exchange with the bulk cytosolic pool; this remains the case, even on timescales up to 30 minutes (not shown).

Sec16A is localised at ERES independently of Sec23-Sec24 and Sec13-Sec31

To confirm that Sec16A has a role at ERES upstream of COPII-subunit association, we wished to define the localisation and kinetics of Sec16A in the absence of other COPII proteins, Sec23-Sec24 and Sec13-Sec31. We had previously noted that very high level overexpression of TBC1D20, a GTP-activating protein for Rab1 and Rab43 (Haas et al., 2007), removed Sec23-Sec24 and Sec13-Sec31 from the tER. Furthermore, dominant-negative Rab1 mutants have been shown to inhibit COPII budding in vitro (Moyer et al., 2001) and to cause a redistribution of Golgi enzymes back to the ER (Alvarez et al., 2003). However, COPII (Sec13-Sec31) labelling was unaffected by expression of these mutants (Alvarez et al., 2003). It is possible that this is due to an incomplete block of Rab1 function for which overexpression of TBC1D20 provides a more robust inhibition or reflects functional redundancy with Rab43. Cells overexpressing TBC1D20 (see Haas et al., 2007) are characterised by their loss of the Golgi complex, as determined by GM130 labelling; COPI also becomes dissociated from these membranes, and COPII (Sec24 or Sec31 labelling) is lost from juxtanuclear ERES; at the highest levels of expression, Sec23-Sec24 and Sec13-Sec31 are also lost from peripheral ERES. Upon very high levels of expression of TBC1D20, the Golgi is indeed severely disrupted (Fig. 4A, GM130 labelling), but although Sec16A remained localised to puncta throughout the cytoplasm (Fig. 4A), the localisation of Sec23-Sec24 (Fig. 4B) and Sec13-Sec31 (Fig. 4C) to the tER membrane at peripheral sites was lost. Similarly, COPI labelling was lost from all peripheral and Golgi membranes (Fig. 4D). It must be noted that these effects on Sec24 and Sec31 localisation only occur upon high-level expression of TBC1D20. At lower levels, only the Golgi is affected (Haas et al., 2007) (note the cell labelled with an arrow in Fig. 4B). A catalytically inactive mutant of TBC1D20 (R105A) had no effect on Golgi or COPII localisation even at very high expression levels (data not shown) (see also Haas et al., 2007). From this, we conclude that human Sec16 does not require the membrane localisation of Sec23-Sec24 or Sec13-Sec31 for its recruitment or sustained localisation to tER.

Recycling kinetics of Sec16A at ERES are unaffected by loss of COPII subunits from tER sites

Quantitative FRAP analysis on cells overexpressing TBC1D20 show no statistically significant difference in half-life of GFP-Sec16A compared with cells expressing the inactive (R105A) mutant of TBC1D20 (P=0.7), or indeed with control cells only expressing GFP-Sec16A (P=0.5) (Fig. 4E). These data suggest that Sec16 can dynamically associate with tER membranes in the absence of other COPII components (Sec23-Sec24 and Sec13-Sec31). Fig. 4F shows that a significant fraction of GFP-Sec16A is immobile even following expression of TBC1D20, indicating that Sec23-Sec24 and Sec13-Sec31 are not required to maintain this population. A slight decrease in the immobile fraction of Sec16 was seen compared with controls that do not express TBC1D20 (Fig. 4, ~35% versus ~40%) but this was not statistically significant (P=0.5). We conclude from this that gross perturbation of Rab function at the ER-Golgi interface does not affect Sec16A.

Localisation of Sec16 to tER

During the progress of our own work, minimal regions of Sec16A and Sec16B that are required for tER localisation were described (Bhattacharyya and Glick, 2007). We found that this region Sec16A (1098-1405, using our numbering) (Bhattacharyya and Glick, 2007), did not in fact localise to tER in HeLa cells and nor did the equivalent construct of Sec16B (data not shown). Although the minimal region previously identified showed some very weak affinity for cytoplasmic puncta that were consistent with tER, with predominant localisation to the nucleus, the localisation was not at all efficient (not shown). Sec16L described by Glick and colleagues (Bhattacharyya and Glick, 2007) is shorter by 178 amino acids at the extreme N-terminus than that we have previously described (Watson et al., 2006) (Sec16A, which corresponds to the previously deposited sequence KIAA0310, NCBI accession numbers NM_014866/NP_055681). We believe that the 2357 amino acid

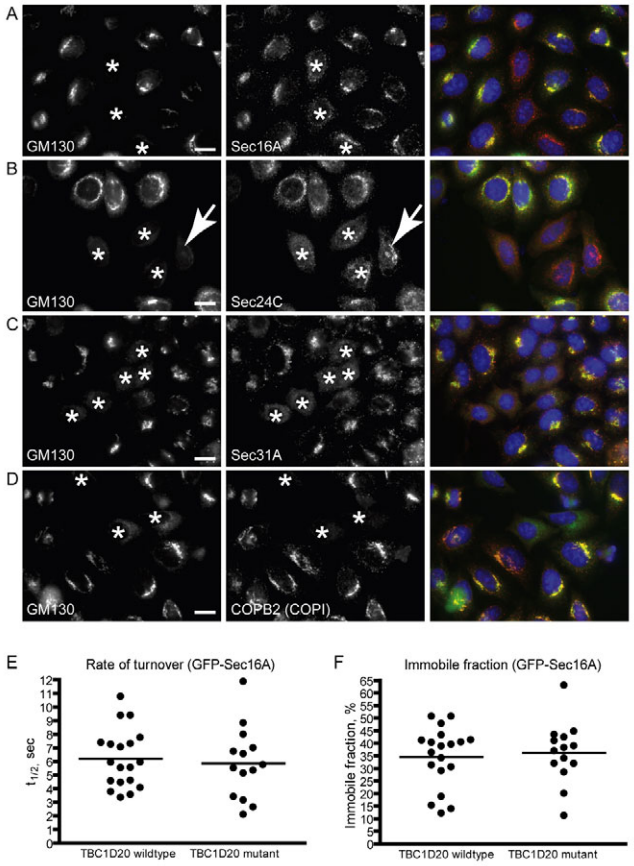

Fig. 4. Association of Sec23-Sec24 and Sec13-Sec31 with ERES membranes is not required to maintain the association of Sec16. (A-D) HeLa cells were transfected with Myc-TBC1D20 and fixed after 22 hours. High expressers were immediately identified using GM130 staining because TBC1D20 expression results in loss of the Golgi complex (Haas et al., 2007) and by subsequent immunolabelling with anti-Myc antibodies (asterisks). Arrow indicates a cell in which the Golgi is completely disrupted with no apparent effect on juxtanuclear ERES (see Haas et al., 2007). Transfection of the catalytically inactive Myc-TBC1D20-R105A had no effect on Golgi organisation or COPII localisation. Cells were co-stained with antibodies to GM130 and (A) Sec16A, (B) Sec24C, (C) Sec31A and (D) COPI. Scale bar: 20 μm. Cells expressing Sec16A and either wild-type TBC1D20, or a catalytically inactive R105A point mutant were used for FRAP experiments; cells were confirmed to express Myc-TBC1D20 by immunofluorescence after FRAP; 97% of all cells transfected with GFP-Sec16A were also transfected with Myc-TBC1D20. (E) Plot of the half-life of recovery of fluorescence for GFP-Sec16A in cells expressing Myc-TBC1D20 or Myc-TBC1D20-R105A. (F) Plot of immobile population of GFP-Sec16A in the presence of TBC1D20 wild type and mutant expressers. The bar represents the mean with individual data points shown. Data shown represent the mean of at least nine independent experiments.

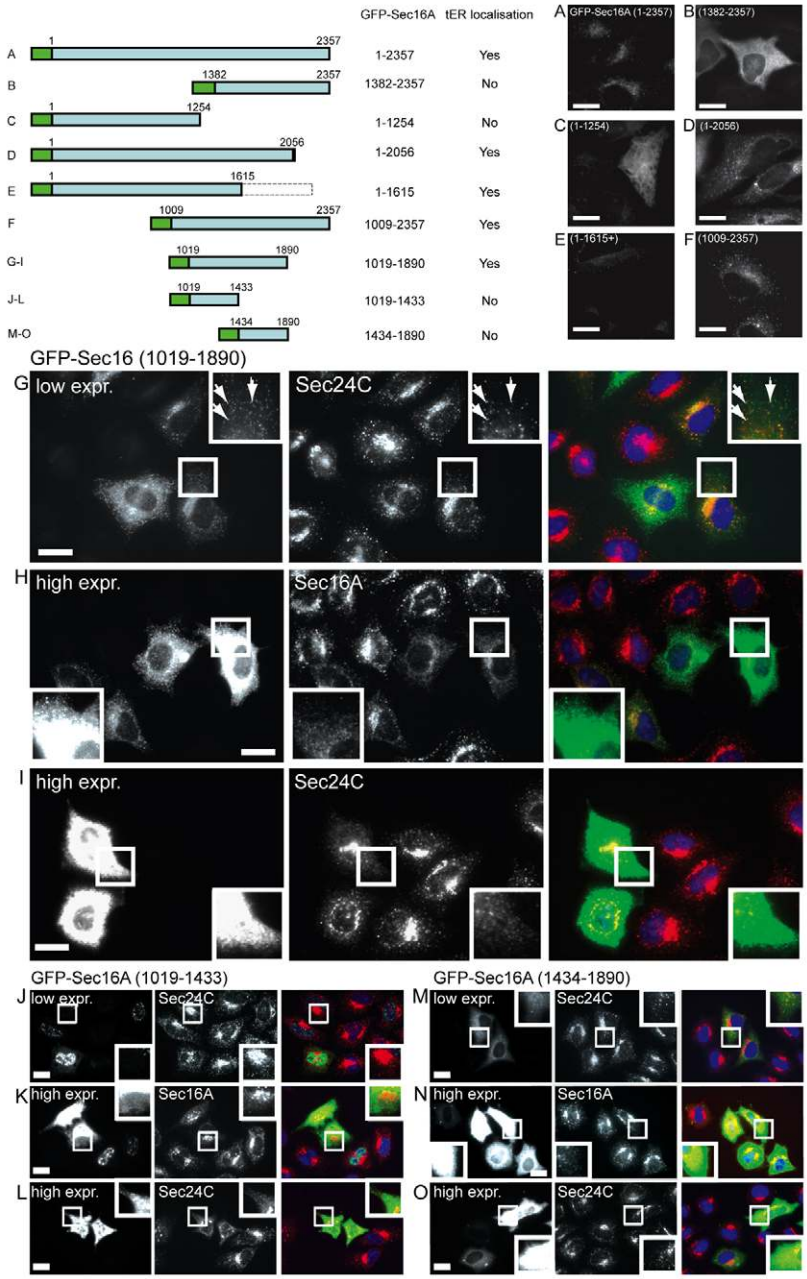

Fig. 5. Requirements for the localisation of GFP-Sec16A in HeLa cells. The top of the figure shows a schematic of constructs generated and summary of findings; lettering refers to both the schematic and micrographs below. Amino acid numbers are shown relative to the full Sec16A (KIAA0310) coding sequence, GFP is indicated by the green bar. Lettering refers to the panels below. (A) Full-length GFP-Sec16A (1-2357) localises to tER. Constructs incorporating regions of Sec16A (see schematic summary) were expressed as GFP-fusion proteins in HeLa cells, fixed and imaged to determine tER localisation. Constructs generated include the following amino acids of Sec16A fused to GFP (B) 1382-2357, (C) 1-1254, (D) 1-2056, (E) 1-1615+, (F) 1009-2357, (G) 1019-1890, (J) 1019-1433 and (M) 1434-1890. (G-I) GFP-Sec16A (1019-1890) efficiently targets to exit sites (G) and shows close apposition to puncta labelled with Sec24C (arrows in the enlargements in G). High expression of GFP-Sec16A (1019-1890) leads to loss of endogenous Sec16A (H) as well as Sec24C (I). (J-L) Sec16A (1019-1433) is not targeted to tER membranes. Low expression of the fusion protein has no effect on Sec24C (J); however, high expression leads to a disruption of Sec16A (K) and Sec24C (L). (M-O) Sec16A (1434-1890) is not targeted to tER membranes and does not cause significant disruption of endogenous Sec16A (O) or Sec24C (N) when highly overexpressed. Scale bars: 20 μm.

form of Sec16A represents the full-length version based on sequence conservation within this extreme N-terminal region with other orthologues, notably those from *Bos taurus*, *Canis familiaris* and *Xenopus laevis*. Throughout, we use the HGNC-approved nomenclature of Sec16A and Sec16B, which is consistent with that used for all other COPII subunits and numbering according to the 2357 amino acid form.

GFP-Sec16A localises faithfully to tER at low to moderate levels of expression (Watson et al., 2006) and Fig. 5A. A series of deletion constructs of Sec16A were then examined for their ability to target to tER. Localisation was compared at high magnification with GFP-Sec16A (1-2357) (Fig. 5A), i.e. the full coding sequence fused to GFP. We found that the C-terminal half of Sec16A (residues 1382-2357) failed to localise to tER and was seen to be predominantly cytosolic (Fig. 5B). Residues 1-1254, approximately the N-terminal half of Sec16A missing the entire CCD and much of the tER localisation domain predicted by Glick and colleagues (Bhattacharyya and Glick, 2007), failed to target to tER but showed a weak ER-like labelling that included clear nuclear envelope labelling (Fig. 5C) and showed significant overlap with the ER marker calnexin (data not shown). Deletion of the C-terminal conserved domain that interacts with Sec23 (Bhattacharyya and Glick, 2007) did not significantly affect this targeting to peripheral tER but resulted in a noted loss of labelling of juxtanuclear structures (1-2056) (Fig. 5D). A shorter construct, including the entire N-terminus and around half of the CCD (1-1615), resulted in targeting to some puncta (Fig. 5E) but these did not label with other COPII proteins (Sec24C, data not shown) and bore little resemblance to tER labelling in control cells. These data show that constructs that lack the CCD fail to target to tER.

Further work has shown that a highly charged sequence N-terminal to the CCD was also required for tER targeting. In

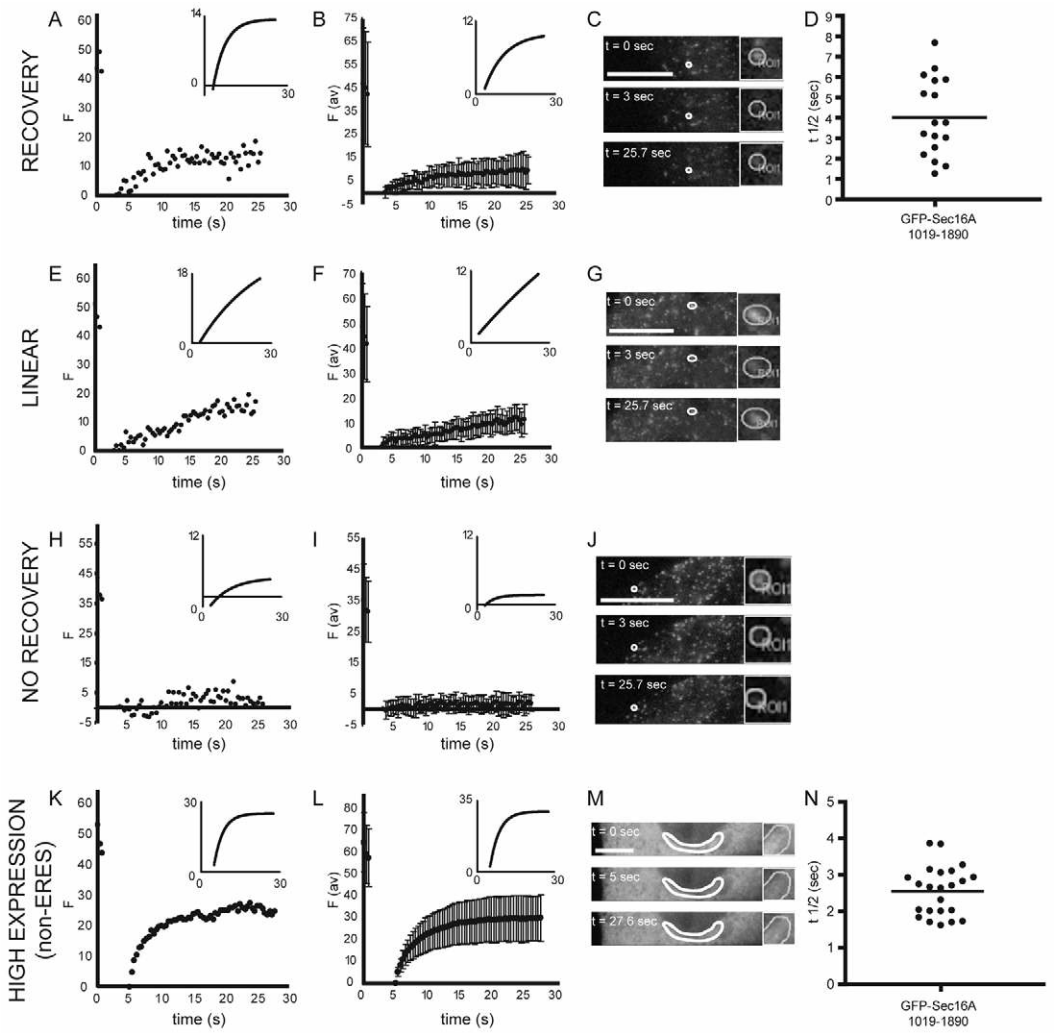

Fig. 6. Fluorescence recovery after photobleaching of GFP-Sec16A (1019-1890). HeLa cells were transfected with GFP-Sec16A (1019-1890) and FRAP was performed on single ERES (A-J) and high-expressing cells (non-ERES) (K-N). Single ERES were found to fall into three populations: one showing recovery (A-D), a second recovering at a slow linear rate (E-G), and a third population showing no recovery (H-J). (A,E,H) Recovery curves of single ERES; insets show data fitted to a single exponential. (B,F,I) Average recovery curves; insets show data fitted to a single exponential. (C,G,J) For each single ERES, images were taken before the bleach (t=0 seconds), immediately after the bleach (t=3 seconds) and at the end of the time course (t=25.7 seconds). Scale bar: 10 μm. (D) Half-life of GFP-Sec16A (1019-1890). Each point represents the half-life of a single ERES, the bar represents the mean. (K-M) Photobleaching of cells highly expressing GFP-Sec16A (1019-1890). The recovery curve of a single ROI and the resulting curve fit (inset) is shown in K. Images acquired before, immediately after the bleach and at the end of the time course are shown in M. Scale bar: 10 μm. In L, the average recovery curve of 23 experiments as well as the curve fit (inset) is displayed. (N) Half-life of GFP-Sec16A (1019-1890) in high-expressing cells. Each point represents the half-life of a single ROI, the bar represents the mean. F, fluorescence intensity; F(av), the mean. Error bars show s.d. See also Table 1.

agreement with the work of Ivan and co-workers (Ivan et al., 2008), we found that an extensive sequence was required here for robust tER localisation; sequence alignment of orthologues showed that this charged region extends to residue 1019 [approximately equivalent to the start of the 'NC2.3.4-CCD' construct used by Ivan and colleagues (Ivan et al., 2008)]. Deletion of the N-terminal 1008 amino acids (leaving 1009-2357) did not significantly affect ERES targeting of Sec16A (Fig. 5F); the N-terminal 1008 amino acids are therefore not involved in targeting of Sec16 to tER and we have yet to be able to ascribe a function to them.

We then mapped the region required for targeting to ERES in more detail. A construct encoding amino acids 1019-1890 (ending at the end of the CCD) efficiently targeted to tER when transiently expressed in HeLa cells (Fig. 5G). Notably, this fusion protein showed close apposition to other COPII markers as we saw for native Sec16A (Fig. 1). At high expression levels GFP-Sec16A (1019-1890) caused a loss of Sec16A-labelled (Fig. 5H), Sec24C-labelled (Fig. 5I), and Sec31A-labelled (not shown) puncta from cells. We subsequently found that the highly charged region incorporating residues 1019-1433 showed robust localisation to the nucleus (Fig. 5J) and only at very high levels of overexpression, at which there is a substantial cytosolic pool, did we observe any perturbation of Sec16A or Sec24C localisation (Fig. 5K,L). GFP-Sec16A (1434-1890), which contains the CCD of Sec16A, showed a strong association with ER membranes (Fig. 5M-O, particularly evident in the enlargement where one can see clear nuclear envelope labelling). This region on its own was also insufficient to disrupt Sec16A or Sec24C localisation (Fig. 5N,O). Thus, we conclude that both the charged region (1019-1433) and the CCD (1434-1890) are required for efficient targeting of Sec16 to tER

Table 1. Fluorescence recovery after photobleaching of GFP-Sec16A

Outcome	Number	$t_{1/2}$ (seconds)	Rate (second^{-1})	Immobile fraction
Recovery	17/48	5.24	n/a	79.6%
Linear	13/48	n/a	0.46	n/a
No recovery	18/48	n/a	n/a	94.8%
High expression	23 cells	2.5	n/a	54%

Results shown are from FRAP experiments on single ERES and in high-expressing cells. Single ERES were found to recover in three distinct populations. The number of ERES per population or the number of high-expressing cells are given as well as the half-life (determined from average of each data set, see Fig. 6B,L) and the immobile fraction. These values differ slightly from those calculated from individual ERES (Fig. 6D,N) because curves are fitted to a single exponential after averaging. The appropriate recovery curves are shown in Fig. 6. n/a, not applicable.

(Fig. 5G; compare to Fig. 5J,M) and disruption of COPII localisation. These data show that the primary site of action of Sec16 is indeed the tER membrane, consistent with its steady state localisation and turnover kinetics.

Since the localisation of amino acids 1019-1890 of Sec16A recapitulates that of the full-length protein, we sought to define whether the truncated construct showed the same kinetics of cycling on and off the membrane, a likely correlate of function. The results of these experiments are shown in Fig. 6 and Table 1. We observed three distinct classes of kinetics of GFP-Sec16A (1019-1890) in FRAP experiments: partial recovery of fluorescence into the bleached area (Fig. 6A-D), linear recovery (Fig. 6E-G), or no recovery of fluorescence (Fig. 6H-J). Fig. 6 shows data for individual ERES and averaged data (both including curves fitted to a single exponential as well as example images from confocal micrographs). Notably (as shown in Table 1), those sites that showed partial recovery did so with relatively similar kinetics to full-length GFP-Sec16A ($t_{½}$=5.24 seconds); a notable distinction to the full-length protein was the presence of a much greater immobile fraction (79.6%) compared with full-length Sec16A (43%). As described in Table 1, recovery was only observed for 17 of 48 ERES examined. Of these 48 sites, 13 showed linear recovery of photobleaching. The absence of a defined end-point meant that it is not appropriate to fit these data to a single exponential and so neither the half life or immobile fraction could be calculated; the linear rate of fluorescence recovery was 0.46% second^{-1}. The remaining 18 of 48 ERES showed no recovery during the experimental period. The initial phase suggests some recovery of fluorescence (at most a few percentage points) but this is on a time scale that was too rapid (or potentially too insignificant) to fit to a single exponential. As shown in Fig. 5, localisation of Sec16A (1019-1890) to ERES is saturable with the overexpressed protein readily localising to the entire ER membrane in fixed cells. Defining the kinetics of turnover of the highly overexpressed construct at ERES versus the ER membrane was precluded by the extensive cytosolic pool of this fusion protein when overexpressed at these levels (this pool would be extracted by methanol fixation). Fig. 6K-N shows FRAP data for this overexpression phenotype, which largely reflects a combination of cytosolic diffusion and ER membrane diffusion. The half-life of recovery here was 2.5 seconds, with an immobile fraction of 54%. This is consistent with the data above and with saturable localisation of this construct to ERES and on higher expression of localisation to the ER in general.

Sec16 CCD interacts with Sec13

Previous work has shown that the C-terminal conserved domain of mammalian Sec16A binds to Sec23 (Bhattacharyya and Glick, 2007); extrapolating from work using the *S. cerevisiae* orthologue would predict further binding sites for other COPII subunits on Sec16A. We therefore undertook both a directed two-hybrid analysis and complete two-hybrid screen using the central conserved domain of Sec16A; we used this domain because it efficiently targets to the ER membrane, suggesting that it might be a likely candidate to identify any protein directing ER localisation. We screened a human adult mixed cDNA library (normalised for message abundance) using the central conserved domain of Sec16A. Sixty clones were isolated that grew on quadruple dropout selection medium. Following plasmid isolation and retransformation, 12 failed to grow, one showed strong interaction both with lamin (a negative control used in all co-transformations) and the CCD of Sec16A, and 47 showed specific interaction between bait and prey. DNA sequencing revealed that all 47 of these clones included the full coding sequence of Sec13, represented by six independent cDNAs. All included at least part of the 5′ and 3′ untranslated regions of the mRNA. Notably, five out of six of these inserts were out of frame, yet showed a strong and specific interaction with the CCD of Sec16A, and activated all reporters in the system. This is probably due to frameshifting during translation in yeast, which has been previously described (Fromont-Racine et al., 1997; Ivanov and Atkins, 2007). We confirmed this interaction by re-cloning the coding region of only Sec13. In addition, we chose to test the ability of the CCD of Sec16 with other COPII components in a directed two-hybrid analysis. These data (Fig. 7) showed that the Sec16 CCD interacted only with Sec13 and not with Sec12, Sar1, Sec23, Sec24 or Sec31. These data also show that the CCD of Sec16A is not responsible for its oligomerisation. This interaction of Sec16A with Sec13 strongly supports the concept of Sec16 as a template or organiser of COPII assembly.

Discussion

The major finding that we present here is that at steady state in human cells, Sec16A frequently localises to regions of ERES that are discrete from other (downstream) COPII components, Sec23-Sec24 and Sec13-Sec31. This is illustrated schematically in Fig. 8; note that this diagram represents the predominant steady-state localisation of these components. It is clear that Sec16 binds to Sec23-Sec24 and also to Sec13-Sec31 (Bhattacharyya and Glick, 2007; Iinuma et al., 2007) (and this study). The localisation of Sec16A, and indeed the other COPII subunits, is also distinct from the ERGIC (labelled with ERGIC-53). Thus Sec16A, the other COPII subunits Sec23, Sec24, Sec13, and Sec31, and ERGIC-53 provide three distinct markers of discrete subcompartments of an ERES (tER, COPII coated vesicles and the ERGIC). The definition of steady-state localisations of these proteins provides an opportunity to fully define the localisation of proteins during exit from the ER or when they become trapped during export, for example through mutation of export motifs (Nishimura and Balch, 1997) or inhibition of oligomerisation (Sato and Nakano, 2003).

The discrete steady-state localisation of Sec23-Sec24 from that of Sec16 is consistent with work from Klumperman and colleagues,

which shows that the majority (72%) of Sec23 or Sec31 labelling in thick EM sections is in fact associated with vesicular and small tubular structures that are not associated with the ER cisterna (Zeuschner et al., 2006). Indeed, within an individual ERES, these authors defined 81% of COPII labelling associated with structures that are not connected to the ER. The study of Zeuschner and co-workers (Zeuschner et al., 2006) did reveal COPII labelling associated with both ER cisterna and budding vesicles that were continuous with the underlying ER, but even when only considering the COPII label within ERES, this accounts for only 18% of the label (Zeuschner et al., 2006). This is entirely consistent with our findings. Previous work has shown that budding profiles within ERES include tubular structures extending ~200 nm from the underlying ER membrane (Bannykh et al., 1996; Bannykh and Balch, 1997). These data showed that a single ERES was made up from multiple independent tubules of ER membrane. The images presented by Bannykh et al. (Bannykh et al., 1996) include some curved regions of ER, and it is possible that we are observing the same structures in our study. This leads to the possibility that one function of Sec16 is to organise these sites, possibly through its oligomerisation (Bhattacharyya and Glick, 2007).

In agreement with these studies, our results suggest that Sec16A localises to cup-like regions of the ER membrane that can be defined as tER, with Sec23-Sec24 (and Sec13-Sec31) showing a primary steady-state localisation to budded, post-ER membranes. This is consistent with the properties of the *Drosophila* orthologue (Ivan et al., 2008). It remains to be determined whether Sec16 localises to these regions because they are cup-shaped, or whether it in fact has a more direct role in generating this curved membrane structure. Both isoforms of Sec16 in humans have the capacity to oligomerise with one another (Bhattacharyya and Glick, 2007). We cannot detect any high order oligomers of Sec16A in cytosol using density gradient centrifugation (data not shown), which supports the notion that oligomerisation occurs on the tER membrane (Ivan et al., 2008),

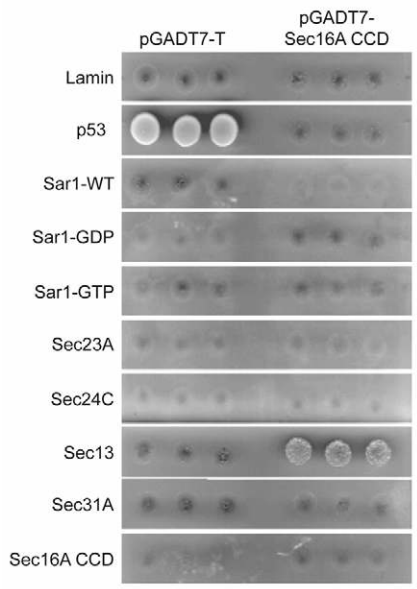

Fig. 7. Interaction of Sec16A CCD and Sec13. (A) Triplicate spots of yeast co-transformed with pGADT7-T (left) or pGADT7-Sec16A CCD (right) and COPII subunits as indicated were plated onto quadruple dropout medium and assayed for growth after 4 days. A positive interaction is seen only between large T antigen (pGADT7-T) and p53 (positive control) and between Sec16A CCD and Sec13. All colonies grow on double dropout medium (not shown).

potentially modulating the properties of Sec16 itself. Evidence from *S. cerevisiae* indicates that Sec16 becomes incorporated into budded vesicles (Espenshade et al., 1995) and similar results in *Drosophila* showed that Sec16 localises at steady state to tubulovesicular membranes that also label with antibodies directed against Sec23 (Ivan et al., 2008). In our EM sections, some labelling for Sec16 is indeed found to be associated with structures that are consistent with COPII vesicles, and around 14% of structures show colocalisation of Sec16 and Sec31 (these measurements were made on groups of particles only, excluding individual gold particles). It is likely that assembly and budding events are rapid, with perhaps a longer residency for some subunits (Sec23, Sec24, Sec13 or Sec31) on budded vesicles, consistent with the notion that the assembled coat acts as a platform for downstream events such as recruitment of tethers (Cai et al., 2007) and motors (Watson et al., 2005). The high rate of recycling of GFP-Sec16A on and off the membrane remains unclear, but would be consistent with a transient incorporation into budded vesicles.

This could reflect a key difference in the mode of action of Sec16 between species, but more probably simply reflects different kinetics of Sec16 assembly and disassembly resulting in different steady-state populations. Given the conservation of the mechanism of COPII-dependent export between species (accepting differences in organisation), this distinction in steady-state localisation indicates that Sec16 might not stably incorporate into COPII vesicles in the way that Sec23-Sec24 and Sec13-Sec31 do. There is a wealth of data implicating Sec16A in COPII-dependent budding from the ER, and consequently, it is pertinent to reiterate that these are the steady-state localisations of these subunits.

Our data further elucidate the mechanism by which human Sec16A is localised to the tER. Using a series of fusion proteins encompassing different regions of Sec16A, we found that both the reported tER localisation domain and the CCD (encompassing amino acids 1019-1890) are required for efficient and robust tER localisation of Sec16A. Furthermore, we found that the targeting of GFP-Sec16A (1019-1890) was saturable, which is consistent with binding to a membrane receptor that is limiting the overexpression of the GFP-Sec16A fusion. Recently, Ivan and colleagues showed that the previously reported region (Bhattacharyya and Glick, 2007) only functions as a tER localisation domain in the presence of the CCD. As indicated by Rabouille and colleagues (Ivan et al., 2008), this region upstream of the CCD includes several highly conserved positively charged residues leading to speculation that membrane

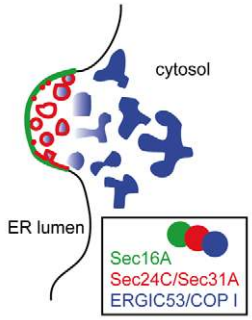

Fig. 8. Schematic of an ERES. At steady state, Sec16 localises to tER (green), Sec23-Sec24 (and also Sec13-Sec31) predominantly localise to post-ER structures (red), and ERGIC-53 to the pre-VTC and ERGIC (blue). These data demonstrate steady-state localisations; functionally considerable overlap will occur (i.e. Sec16 can bind directly to Sec23-Sec24, and Sec23-Sec24 mediates the export of cargo from the ER including ERGIC-53).

association via this region could be mediated through interaction with polar phospholipids.

Our data also show that the localisation of Sec16A is independent of the presence of Sec23-Sec24 and/or Sec13-Sec31 on ERES membranes. This is in agreement with recent findings on *Drosophila* Sec16 (Ivan et al., 2008). This demonstrates that despite the clear difference in intracellular organisation, the individual components of the COPII machinery are indeed closely related between species. At first, it would appear that one clear difference does exist between human and *Drosophila* Sec16. We previously showed that Sar1-GTP mediated the recruitment of Sec16A to membranes (Watson et al., 2006). By contrast, Rabouille and colleagues showed that Sec16 in fact acts to cluster Sar1-GTP at tER (Ivan et al., 2008). It is possible that our initial interpretation was wrong and that in fact the loss of Sec16A we observed upon expression of a GDP-restricted mutant of Sar1 (Watson et al., 2006) could result from indirect effects of blocking COPII-dependent transport. However, our interpretation was also based on the robust assembly of Sec16 into curved structures within cells upon co-expression of GFP-Sec16 with Sar1-GTP (Watson et al., 2006). An alternative explanation is that, rather than promoting its association, Sar1-GTP prevents dissociation of Sec16 from membranes. Full reconciliation of these findings requires further work and a full mechanistic understanding of the mechanisms that specify recruitment of Sec16 to tER membranes.

The accumulated data support the idea that Sec16 acts as a platform to assemble the COPII coat, notably through its binding to Sar1 (Ivan et al., 2008), to Sec23 (Bhattacharyya and Glick, 2007) and to Sec13 (this study). The large immobile population of Sec16A seen in FRAP experiments (Stephens et al., 2000; Forster et al., 2006) (and this study) is likely to be significant for its role as a template for COPII assembly. The interaction of Sec16 with Sec13 could modulate the recruitment of Sec13 to ERES, provide an additional binding site to retain Sec13-Sec31 in the vicinity of budding sites or act directly in the incorporation of Sec13-Sec31 into the COPII vesicle coat. In summary, our data define markers that discriminate between subcellular structures that could be used to define the point at which membrane trafficking is arrested in experimental systems and clinically relevant states.

Materials and Methods

Reagents

All chemical reagents were purchased from Sigma unless stated otherwise. HeLa cells were grown in DMEM containing 10% fetal calf serum (Invitrogen, Paisley, UK). For immunofluorescence, cells were grown on 22 mm coverslips, fixed with methanol at –20°C for 4 minutes and immunolabelled as described (Stephens et al., 2000).

Plasmids and cDNA construction

Myc-TBC1D20 and GFP-Sec16A have been described previously (Haas et al., 2007; Watson et al., 2006). The reported tER localisation domains of Sec16L (Sec16A) and Sec16S (Sec16B) were obtained from Ben Glick (University of Chicago, IL) and are described elsewhere (Bhattacharyya and Glick, 2007). Subregions of Sec16A and Sec16B were generated according to standard molecular biology protocols and fused to EGFP using pEGFP-C1 or pEGFP-C2 (Clontech, Mountain View, CA).

Antibody reagents

Antibodies used were as follows: anti-Sec16 (KIAA0310, Bethyl labs), anti-Sec23A rabbit polyclonal (Affinity Bioreagents, Golden, CO), anti-calnexin (BD Biosciences), anti-ERGIC-53 (Sigma), anti-Sec31A (BD Biosciences, Cambridge, UK), anti-COP β′ mAD (Sigma), and Sec24C (Townley et al., 2008). Primary antibodies were detected by using anti-mouse, anti-rabbit or anti-sheep secondary antibodies conjugated to Alexa Fluor 568 or Alexa Fluor 647 (Invitrogen).

Scanning confocal microscopy, Nyquist sampling and deconvolution

Cells were imaged using Leica TCS-SP5 AOBS scanning confocal microscope and processed using Photoshop 6.0 (Adobe, Uxbridge, UK) and montages generated using Adobe Illustrator (Adobe). To provide the highest degree of accuracy, Nyquist sampling theorem was applied to ascertain the correct voxel size for sampling the image. The Nyquist sampling theorem states the optimum pixel size for sampling the image is at least ½ spatial resolution. This translates to 11.2 samples per μm or a maximum distance of 89 nm pixel width. To adjust to this criteria, a higher pixel number (1024×1024) and zoom factor (×5.4) was used. For GFP-Sec16A the calculated pixel size used was 43×43×130 (x, y, z in nm). Furthermore, to mimic the maximum spatial bandwidth criterion imposed by Nyquist reconstruction, images in Fig. 1 underwent iterative deconvolution to fit the data acquired to the required image resolution.

For GFP-Sec16A the calculated pixel size used was 43×43×130 (x, y, z in nm) (http://support.svi.nl/wiki/NyquistCalculator). Deconvolution was performed using Volocity 4.2 (Improvision, Coventry, UK) with an iterative deconvolution algorithm specifying an iteration limit of 25, and a confidence level of 98%. Point Spread Functions were calculated using Volocity 4.2.

Immunoelectron microscopy and tomography

Immunoelectron microscopy was performed as described previously (Scheiffele et al., 1998) with the following modifications. Confluent HeLa cells were fixed with 2% paraformaldehyde and 0.05% glutaraldehyde in phosphate buffer. Cells were pelleted in 12% gelatin and cryo-protected with 2.3 M sucrose. Immunolabelling was performed on 70 nm cryosections collected on carbon-coated copper grids. Grids were incubated for 1 hour with polyclonal rabbit anti-Sec16A (1:15) and monoclonal mouse anti-Sec31A (BD Biosciences, 1:100) in 0.1% acetylated BSA in PBS. After rinsing in PBS, grids were incubated for 1 hour with anti-mouse IgG coupled to 10 nm gold particles and anti-rabbit IgG coupled to 6 nm gold particles. Sections were examined in a Philips CM100 transmission electron microscope. For quantification, 74 images of three independent experiments were taken from the juxtanuclear area. All gold particles were counted and distances measured. Groups were defined as more than three colocalising particles. To control the quantification and exclude effects of differential staining efficiency, gold particle sizes were swapped for secondary antibodies in a separate experiment and counted the same way (25 images); results obtained were comparable. For electron tomography, ~210-nm-thick cryosections were immunolabelled as above. Tilt series from –70° to +70° were acquired on a FEI Tecnai 20, 200 kV TEM (FEI Company, Eindhoven, The Netherlands) using the FEI tomography acquisition software (Xplore3D) and a single tilt tomography holder (Fischione, Export, PA). The tilt series was reconstructed using Inspect3D (FEI Company) and modeled in ResolveRT (FEI-licensed version of AMIRA, Mercury Computer Systems, Chelmsford, MA).

TBC1D20 overexpression

HeLa cells were transfected with TBC1D20 (Haas et al., 2007) using Fugene6 (Roche Biochemicals, Burgess Hill, UK) according to the manufacturer's instructions. Cells were imaged using LeicaTCS-SP5 AOBS scanning confocal microscope and images processed using Photoshop 6.0 (Adobe, Uxbridge, UK) and montages generated using Adobe Illustrator 10 (Adobe).

Fluorescence recovery after photobleaching and analysis

Cells grown on live cell dishes (MatTek, Ashland, MA) were imaged at 37°C with the microscope LeicaTCS-SP5 AOBS scanning confocal microscope enclosed in a heated Perspex box in DMEM without phenol red, supplemented with 30 mM HEPES, pH 7.4, 0.5 g/l sodium bicarbonate and 10% fetal calf serum. For quantitative FRAP measurements a 63× 1.4 NA Plan-Apochromat objective was used. Photobleaching of GFP was performed with a ~500 nm diameter circular region. Pre- and post-bleach images were collected for 30 seconds using 15% AOTF power, 20% laser intensity. For GFP-Sec16A and GFP-Sec23A FRAP was performed on HeLa cells using a pinhole size of 6 Airy units, at 1 frame every 0.215 seconds, and region-of-interest bleaching with five iterations of the 488 and 514 nm lasers at 100% AOTF power. For GFP-Sec16A (1019-1890), a pinhole size of 4 Airy units, a scan rate of 1 frame every 0.38 seconds, twofold line averaging, and region-of-interest bleaching with five iterations for low expressing cells and ten iterations for highly expressing cells of the 476, 488 and 496 nm lasers at 100% AOTF power were used. Background correction was not performed. ERES that moved out of focus or moved over 500 nm during the photobleaching series could not be analysed. Fluorescence recovery in the bleached region during the time series was quantified using Leica LAS-AF FRAP Wizard and exported for analysis to GraphPad Prism 4.02. Recycling kinetics were obtained by curve fitting to a one phase exponential $f(t)=A\times(1-e^{-kt}) + B$, where, A is the mobile fraction, B is the fluorescence directly after photobleaching (%), and k is the rate of fluorescence recovery from which $t_{½}$ is determined [$t_{½}=\ln(2)/k$]. Statistical significance was determined using standard deviation and the Student's unpaired t-test.

Fluorescence loss in photobleaching and analysis

Cells grown on live cell dishes (MatTek) were imaged at 37°C with the microscope Leica TCS-SP5 AOBS scanning confocal microscope enclosed in a heated Perspex box in DMEM without phenol red, supplemented with 30 mM HEPES, pH 7.4, 0.5 g/l sodium bicarbonate and 10% fetal calf serum. For quantitative FLIP measurements a 63× 1.4 NA Plan-Apochromat objective was used. Photobleaching of GFP was

performed within a region-of-interest that encompassed ~40% of the cell cytoplasm. Images were collected for 12 minutes using 15% AOTF power, 20% laser intensity, while bleaching the region-of-interest intermittently with 488 and 514 nm lasers at 100% AOTF power. FLIP was performed on HeLa cells using a pinhole size of 6 Airy units, at 1 frame per second. Background correction was not required. Fluorescence loss outside of the bleached region during the time series was quantified using Volocity 4.2 (Improvision, Coventry, UK) tracker and exported for analysis to Microsoft Excel 2000.

Yeast two-hybrid screen

The yeast two-hybrid screen was performed using the pre-transformed Normalized Matchmaker human universal cDNA Library containing $>1\times10^6$ independent clones (Clontech). The synthesised cDNA has been normalised for abundance before library construction using the prey vector pGADT7-RecAB. The amino acid sequence of Sec16A (1434-1890) was cloned into the bait vector pGBKT7 (Clontech) using *Eco*RI and *Bam*HI. Following transformation of the bait plasmid into the yeast AH109, the two hybrid screen was performed by yeast mating with the pretransformed library strain (Y187) according to the manufacturer's instructions. 6×10^6 clones were screened. The mated yeast were plated on synthetic dropout medium (–Ade/–His/–Leu/–Trp) containing 2 mM 3-aminotriazole and grown for 10-14 days at 30°C. After re-plating of the colonies on to fresh SD –Ade/–His/–Leu/–Trp containing 2 mM 3-AT and 40 μg/ml X-α-Gal, the library plasmids from putative positive interactors were isolated. These were further verified by co-transformation of the library plasmid with the bait construct or lamin as negative control. Only clones showing a positive interaction with the bait, but not with lamin, were identified by sequencing (Eurofins MWG Operon, Germany).

Directed yeast two-hybrid assays

Interactions were evaluated by co-transformation of bait pGADT7-Sec16A-CCD (1434-1890) with COPII components cloned into pGBKT7. pGBKT7-lamin + pGADT7-Sec16A (1434-1890) acted as negative control, and pGBKT7-p53 + pGADT7-T as positive control. Co-transformations were plated onto synthetic dropout medium (–Ade/–His/–Leu/–Trp) and positive interactions were identified using X-α-gal.

We would like to thank Harry Mellor, Jon Lane, Nigel Savery, Mark Dillingham, Mark Szczelkun, Pete Cullen, and members of the Stephens laboratory for helpful advice and discussions, and Jeremy Rees of FEI Company for assistance with tomographic reconstructions. We thank the MRC for funding this work through a Senior Non-Clinical Fellowship (to D.J.S., G117/553), and the BBSRC for a research grant (BB/E019633) and doctoral training account studentships. We are also grateful to the University of Bristol, MRC and Wolfson Foundation for providing generous support to establish and develop the Wolfson Bioimaging Facility. Deposited in PMC for release after 6 months.

References

Alvarez, C., Garcia-Mata, R., Brandon, E. and Sztul, E. (2003). COPI recruitment is modulated by a Rab1b-dependent mechanism. *Mol. Biol. Cell* **14**, 2116-2127.

Antonny, B., Madden, D., Hamamoto, S., Orci, L. and Schekman, R. (2001). Dynamics of the COPII coat with GTP and stable analogues. *Nat. Cell Biol.* **3**, 531-537.

Appenzeller-Herzog, C. and Hauri, H. P. (2006). The ER-Golgi intermediate compartment (ERGIC): in search of its identity and function. *J. Cell Sci.* **119**, 2173-2183.

Bannykh, S. I. and Balch, W. E. (1997). Membrane dynamics at the endoplasmic reticulum-Golgi interface. *J. Cell Biol.* **138**, 1-4.

Bannykh, S. I., Rowe, T. and Balch, W. E. (1996). The organization of endoplasmic reticulum export complexes. *J. Cell Biol.* **135**, 19-35.

Bhattacharyya, D. and Glick, B. S. (2007). Two mammalian Sec16 homologues have nonredundant functions in endoplasmic reticulum (ER) export and transitional ER organization. *Mol. Biol. Cell* **18**, 839-849.

Bielli, A., Haney, C. J., Gabreski, G., Watkins, S. C., Bannykh, S. I. and Aridor, M. (2005). Regulation of Sar1 NH2 terminus by GTP binding and hydrolysis promotes membrane deformation to control COPII vesicle fission. *J. Cell Biol.* **171**, 919-924.

Cai, H., Yu, S., Menon, S., Cai, Y., Lazarova, D., Fu, C., Reinisch, K., Hay, J. C. and Ferro-Novick, S. (2007). TRAPPI tethers COPII vesicles by binding the coat subunit Sec23. *Nature* **445**, 941-944.

Connerly, P. L., Esaki, M., Montegna, E. A., Strongin, D. E., Levi, S., Soderholm, J. and Glick, B. S. (2005). Sec16 is a determinant of transitional ER organization. *Curr. Biol.* **15**, 1439-1447.

Espenshade, P., Gimeno, R. E., Holzmacher, E., Teung, P. and Kaiser, C. A. (1995). Yeast SEC16 gene encodes a multidomain vesicle coat protein that interacts with Sec23p. *J. Cell Biol.* **131**, 311-324.

Forster, R., Weiss, M., Zimmermann, T., Reynaud, E. G., Verissimo, F., Stephens, D. J. and Pepperkok, R. (2006). Secretory cargo regulates the turnover of COPII subunits at single ER exit sites. *Curr. Biol.* **16**, 173-179.

Fromme, J. C., Ravazzola, M., Hamamoto, S., Al-Balwi, M., Eyaid, W., Boyadjiev, S. A., Cosson, P., Schekman, R. and Orci, L. (2007). The genetic basis of a craniofacial disease provides insight into COPII coat assembly. *Dev. Cell* **13**, 623-634.

Fromont-Racine, M., Rain, J. C. and Legrain, P. (1997). Toward a functional analysis of the yeast genome through exhaustive two-hybrid screens. *Nat. Genet.* **16**, 277-282.

Haas, A. K., Yoshimura, S., Stephens, D. J., Preisinger, C., Fuchs, E. and Barr, F. A. (2007). Analysis of GTPase-activating proteins reveals that Rab1 and Rab43 are key Rabs required for the maintenance of a functional Golgi in human cells.. *J. Cell Sci.* **120**, 2997-3010.

Hammond, A. T. and Glick, B. S. (2000). Dynamics of transitional endoplasmic reticulum sites in vertebrate cells. *Mol. Biol. Cell* **11**, 3013-3030.

Heinzer, S., Worz, S., Kalla, C., Rohr, K. and Weiss, M. (2008). A model for the self-organization of exit sites in the endoplasmic reticulum. *J. Cell Sci.* **121**, 55-64.

Hughes, H. and Stephens, D. J. (2008). Assembly, organization, and function of the COPII coat. *Histochem. Cell Biol.* **129**, 129-151.

Iinuma, T., Shiga, A., Nakamoto, K., O'Brien, M. B., Aridor, M., Arimitsu, N., Tagaya, M. and Tani, K. (2007). Mammalian Sec16/p250 plays a role in membrane traffic from the endoplasmic reticulum. *J. Biol. Chem.* **282**, 17632-17639.

Ivan, V., de Voer, G., Xanthakis, D., Spoorendonk, K. M., Kondylis, V. and Rabouille, C. (2008). Drosophila Sec16 mediates the biogenesis of tER sites upstream of Sar1 through an arginine-rich motif. *Mol. Biol. Cell* **19**, 4352-4365.

Ivanov, I. P. and Atkins, J. F. (2007). Ribosomal frameshifting in decoding antizyme mRNAs from yeast and protists to humans: close to 300 cases reveal remarkable diversity despite underlying conservation. *Nucleic Acids Res.* **35**, 1842-1858.

Ladinsky, M. S., Mastronarde, D. N., McIntosh, J. R., Howell, K. E. and Staehelin, L. A. (1999). Golgi structure in three dimensions: functional insights from the normal rat kidney cell. *J. Cell Biol.* **144**, 1135-1149.

Lee, M. C., Orci, L., Hamamoto, S., Futai, E., Ravazzola, M. and Schekman, R. (2005). Sar1p N-terminal helix initiates membrane curvature and completes the fission of a COPII vesicle. *Cell* **122**, 605-617.

Martinez-Menarguez, J. A., Geuze, H. J., Slot, J. W. and Klumperman, J. (1999). Vesicular tubular clusters between the ER and Golgi mediate concentration of soluble secretory proteins by exclusion from COPI-coated vesicles. *Cell* **98**, 81-90.

Matsuoka, K., Orci, L., Amherdt, M., Bednarek, S. Y., Hamamoto, S., Schekman, R. and Yeung, T. (1998). COPII-coated vesicle formation reconstituted with purified coat proteins and chemically defined liposomes. *Cell* **93**, 263-275.

Miller, E., Antonny, B., Hamamoto, S. and Schekman, R. (2002). Cargo selection into COPII vesicles is driven by the Sec24p subunit. *EMBO J.* **21**, 6105-6113.

Moyer, B. D., Allan, B. B. and Balch, W. E. (2001). Rab1 interaction with a GM130 effector complex regulates COPII vesicle cis-Golgi tethering. *Traffic* **2**, 268-276.

Nishimura, N. and Balch, W. E. (1997). A di-acidic signal required for selective export from the endoplasmic reticulum. *Science* **277**, 556-558.

Orci, L., Ravazzola, M., Meda, P., Holcomb, C., Moore, H. P., Hicke, L. and Schekman, R. (1991). Mammalian Sec23p homologue is restricted to the endoplasmic reticulum transitional cytoplasm. *Proc. Natl. Acad. Sci. USA* **88**, 8611-8615.

Palade, G. (1975). Intracellular aspects of the process of protein synthesis. *Science* **189**, 347-358.

Ronchi, P., Colombo, S., Francolini, M. and Borgese, N. (2008). Transmembrane domain-dependent partitioning of membrane proteins within the endoplasmic reticulum. *J. Cell Biol.* **181**, 105-118.

Sato, K. and Nakano, A. (2003). Oligomerization of a cargo receptor directs protein sorting into COPII-coated transport vesicles. *Mol. Biol. Cell* **14**, 3055-3063.

Sato, K. and Nakano, A. (2005). Dissection of COPII subunit-cargo assembly and disassembly kinetics during Sar1p-GTP hydrolysis. *Nat. Struct. Mol. Biol.* **12**, 167-174.

Scheiffele, P., Verkade, P., Fra, A. M., Virta, H., Simons, K. and Ikonen, E. (1998). Caveolin-1 and -2 in the exocytic pathway of MDCK cells. *J. Cell Biol.* **140**, 795-806.

Sesso, A., de Faria, F. P., Iwamura, E. S. M. and Correa, H. (1992). A three-dimensional reconstruction study of the rough ER-Golgi interface in serial thin sections of the pancreatic acinar cell of the rat. *J. Cell Sci.* **107**, 517-528.

Stagg, S. M., Gurkan, C., Fowler, D. M., LaPointe, P., Foss, T. R., Potter, C. S., Carragher, B. and Balch, W. E. (2006). Structure of the Sec13/31 COPII coat cage. *Nature* **439**, 234-238.

Stephens, D. J., Lin-Marq, N., Pagano, A., Pepperkok, R. and Paccaud, J. P. (2000). COPI-coated ER-to-Golgi transport complexes segregate from COPII in close proximity to ER exit sites. *J. Cell Sci.* **113**, 2177-2185.

Stinchcombe, J. C., Nomoto, H., Cutler, D. F. and Hopkins, C. R. (1995). Anterograde and retrograde traffic between the rough endoplasmic reticulum and the Golgi complex. *J. Cell Biol.* **131**, 1387-1401.

Tang, B. L., Wang, Y., Ong, Y. S. and Hong, W. (2005). COPII and exit from the endoplasmic reticulum. *Biochim. Biophys. Acta* **1744**, 293-303.

Townley, A. K., Feng, Y., Schmidt, K., Carter, D. A., Porter, R., Verkade, P. and Stephens, D. J. (2008). Efficient coupling of Sec23-Sec24 to Sec13-Sec31 drives COPII-dependent collagen secretion and is essential for normal craniofacial development. *J. Cell Sci.* **121**, 3025-3034.

Watson, P., Forster, R., Palmer, K. J., Pepperkok, R. and Stephens, D. J. (2005). Coupling of ER exit to microtubules through direct interaction of COPII with dynactin. *Nat. Cell Biol.* **7**, 48-55.

Watson, P., Townley, A. K., Koka, P., Palmer, K. J. and Stephens, D. J. (2006). Sec16 defines endoplasmic reticulum exit sites and is required for secretory cargo export in mammalian cells. *Traffic* **7**, 1678-1687.

Weissman, J. T., Plutner, H. and Balch, W. E. (2001). The mammalian guanine nucleotide exchange factor mSec12 is essential for activation of the Sar1 GTPase directing endoplasmic reticulum export. *Traffic* **2**, 465-475.

Zeuschner, D., Geerts, W. J., van Donselaar, E., Humbel, B. M., Slot, J. W., Koster, A. J. and Klumperman, J. (2006). Immuno-electron tomography of ER exit sites reveals the existence of free COPII-coated transport carriers. *Nat. Cell Biol.* **8**, 377-383.